

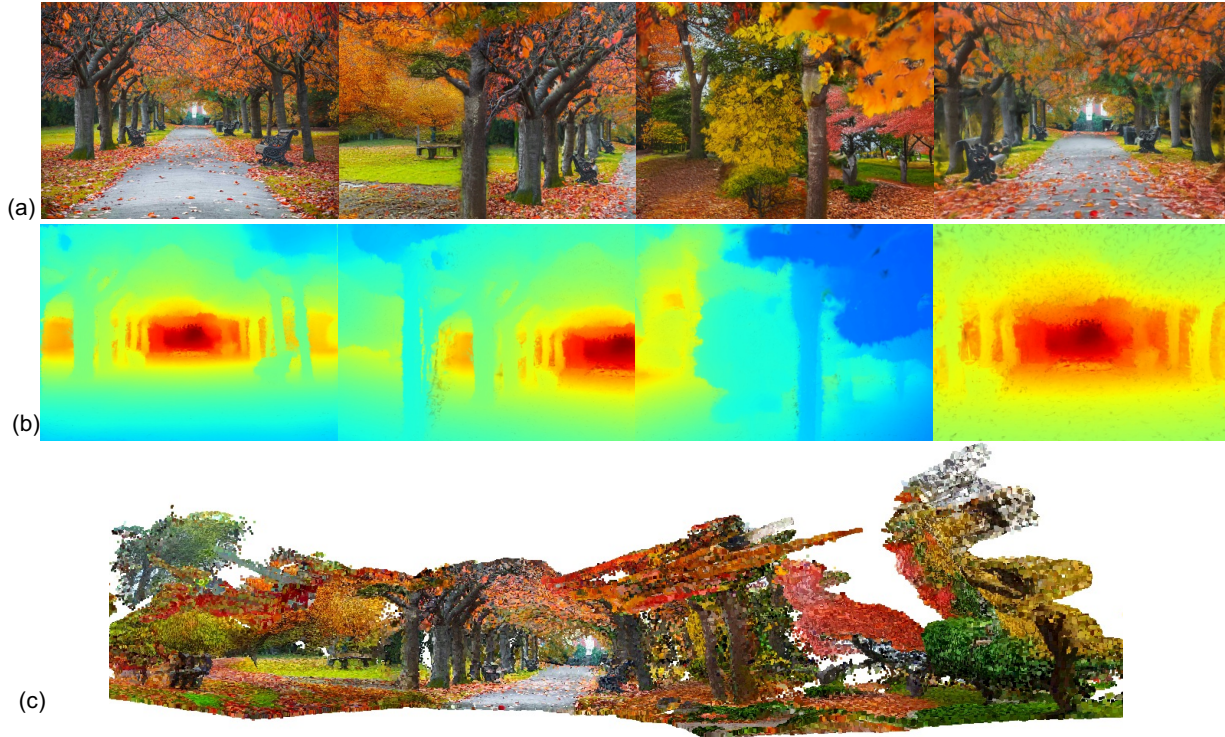
Text2Immersion: Generative Immersive Scene with 3D Gaussians

Hao Ouyang
HKUST

Stephen Lombardi
Google

Kathryn Heal
Google

Tiancheng Sun
Google



Prompt: Autumn Park

Figure 1. **Generation results** of high-fidelity 3D immersive scenery of Text2Immersion pipeline. (a) Examples of renderings, as viewed from four selected directions. (b) Associated depth maps for each view, simultaneously generated by our method. (c) Point cloud demonstrating the global structure of the produced immersive scene, a collection of 3D Gaussian primitives. Shown is only the centers of the Gaussians. To capture the consistency of our generated scenes, we encourage readers to view the accompanying supplementary videos.

Abstract

We introduce *Text2Immersion*, an elegant method for producing high-quality 3D immersive scenes from text prompts. Our proposed pipeline initiates by progressively generating a Gaussian cloud using pre-trained 2D diffusion and depth estimation models. This is followed by a refining stage on the Gaussian cloud, interpolating and refining it to enhance the details of the generated scene. Distinct from prevalent methods that focus on single object or indoor scenes, or employ zoom-out trajectories, our approach generates diverse scenes with various objects, even extending to the creation of imaginary scenes. Consequently,

Text2Immersion can have wide-ranging implications for various applications such as virtual reality, game development, and automated content creation. Extensive evaluations demonstrate that our system surpasses other methods in rendering quality and diversity, further progressing towards text-driven 3D scene generation. We will make the source code publicly accessible at the [project page](#).

1. Introduction

Three-dimensional content generation has numerous potential applications, most notably in gaming, film production, and virtual reality environments. The capability to generate

3D immersive environments that are rich in details can expedite the development of vibrant virtual worlds. Inspired by the recent substantial advancements in 2D generative structures [39] and 3D representations [19, 27], the field of 3D generation has similarly seen rapid progress. However, there still exists a critical gap between 2D and 3D generation. While 2D generation benefits from a wealth of training pairs, the creation of large scale 3D model datasets requires considerable human effort. Consequently, these datasets often suffer from limited diversity and realism, which limits the capability of supervised learning in 3D content generation.

To overcome the prevailing limitation of insufficient training data for 3D generation, innovative solutions with zero-shot text-to-3D generation using pretrained diffusion models have been proposed. Dreamfusion [36] introduced the concept of Score Distillation Sampling (SDS) and distills 3D geometry and appearance from 2D diffusion models, which has significantly influenced the recent evolution of lifting methods in 3D content generation. Despite these significant advances, their generation capabilities remain predominantly constrained to 3D objects of relatively simple geometries. In contrast, an alternative approach, as employed in SceneScape [8], Text2Room [14], and Text2Nerf [53], leverages the color images generated by text-image diffusion models to guide the reconstruction of 3D scenes. However, each of these methods has its limitations. For instance, when using mesh as 3D representation, the generation process is mostly confined to indoor scenes as outdoor environments tend to distort the meshes. Similarly, when utilizing Neural Radiance Fields (NeRF) [27] as a form of 3D representation, the methods encounter challenges with slow rendering speeds and compromised rendering quality due to insufficient supervision.

In this work, we introduce the Text2Immersion framework, a novel approach capable of generating consistently immersive, photorealistic 3D scenes while maintaining real-time rendering speeds. Our method uses 3D Gaussians [19] as the 3D representations for generation, which significantly enhances rendering fidelity and improves 3D details. The proposed pipeline is composed of two stages: coarse 3D Gaussian initialization and 3D Gaussian refinement including inpainting and super-resolution. In the initial stage, we progressively sample coarse anchor cameras and employ text-to-image diffusion models to generate or outpaint the image. Leveraging monocular depth estimation and depth alignment, we project all points to canonical coordinates, thereby constructing the initial coarse Gaussian cloud. A pivotal challenge that arises is the construction of Gaussians from sparse views alone. Drawing inspiration from deep image priors [46], we early stop the optimization process to maintain the rendering quality. We also observe that the training process of Gaussians, particularly with the split-

and-clone operations, serves as a natural adaptive representations. This insight aids in the inpainting Gaussians using only 2D images and the direct super-resolution of Gaussians from 2D supervisions. Through the implementation of these steps, our generated scene achieves both high-fidelity and 3D consistency.

The pipeline proposed in this work can generate 3D photorealistic scenes that maintain consistency across varying text prompts. Each prompt yields a highly diverse set of scenes. These generated 3D scenes correspond well to the text input, as evidenced by high Clip Match scores [12]. Once a scene is generated, it can be rendered at a rate of 180 frames per second on a 3070 laptop GPU. In comparison to other scene generation methodologies, our approach attains a competitive degree of photorealism as shown in Fig. 3. The generation process exhibits robust performance across 360-degree surroundings and even when handling stylized input. Our proposed framework consistently delivers superior 3D consistency and high-fidelity synthesized frames, thus validating its potential as a valuable asset in the domain of 3D scene generation.

2. Related Work

3D Representations Various 3D representations have been investigated for a spectrum of 3D tasks, each posing unique advantages and challenges. Traditional 3D representations, including volume [26, 33], point cloud [2], multiplane images (MPI) [6, 45], and meshes [32], each have distinct disadvantageous aspects when applied to 3D generation tasks. For instance, volume-based methods often entail high memory and computational costs, leading to lower resolution outcomes. Point clouds, while being flexible, fail to achieve photorealistic rendering quality, particularly when point density is insufficient. Generating meshes using neural networks presents a significant difficulty, and MPI is largely restricted to representing front-facing sceneries.

Meanwhile, implicit neural representations, especially Neural Radiance Fields (NeRF) [1, 27], have achieved exceptional rendering quality. However, the optimization of NeRF can be time-consuming and necessitates denser views. While various methodologies have been proposed to accelerate the optimization process, they are effective for reconstruction only. Most recently, the introduction of 3D Gaussian splatting [19] has made a significant impact, demonstrating remarkable quality and speed in 3D reconstruction through an efficient, differentiable renderer. Concurrent works have underscored its substantial potential in 3D object generation [43, 52]. Through this study, we further demonstrate the impressive potential of 3D Gaussians for immersive scene generation.

Text-to-3D generation Generating 3D content has been a long-standing area of research focus. Initial efforts predominantly concentrated on generating 3D shapes within spe-

cific domains, such as automobiles, rooms, and faces [4, 5, 9, 14, 18, 21, 34, 35]. However, due to their inability to accommodate text prompts as input, these early models were limited in application. They lacked both explicit control and the capacity for high-quality texture generation. A number of other preliminary methodologies, including SynSin [50] and PixelSynth [38], initiate from image inputs and directly predict the 3D geometry. As a consequence, the scenes they generate are confined to a limited viewing range around the input image.

The rapid development of text-to-image methods [7, 13, 39, 40, 42] has led a wave of innovation in text-to-3D architectures [10, 11, 16, 17, 31, 48, 49]. However, directly applying 2D generation models to 3D content production still remains challenging, primarily due to the lack of large-scale 3D datasets. Consequently, current feed-forward text-to-3D structures are only able to generate objects within single categories.

To achieve a broader diversity in generation results, researchers have begun to distill 3D information from 2D diffusion models. Early works in this direction, such as CLIPMesh [30], PureCLIPNeRF [20], and DreamFields [15], have leveraged a semantically supervised optimization strategy, under the guidance of a pretrained CLIP model [37], to infer shapes and textures for 3D meshes or NeRF representations. Given the extraordinary generation capabilities demonstrated by the diffusion model, recent approaches [36, 47] have sought to optimize a 3D representation to attain a high likelihood in pretrained 2D diffusion models when rendered from various viewpoints. This strategy ensures both 3D consistency and photorealism. Subsequent works [22, 24, 25, 43, 44, 51] have further enhanced training stability and generation fidelity. However, these studies have primarily concentrated on object-level generation. In contrast, our focus lies in generating immersive virtual reality scenes.

Our research shares significant parallels with recent text-to-scene studies. Works such as Text2Room [14] and SceneScape [8] employ diffusion models for the progressive generation of meshes, which, by consequence, confines the generated scenes primarily to indoor settings; any deviation from this context tends to result in considerable distortion. Conversely, Text2Nerf [53] represents the scene with NeRF [27], enabling a more generalized generation. Our model adopts 3D Gaussians [19], leveraging its inherent priors for multi-stage inpainting and super-resolution. This approach culminates in significantly superior rendering quality, coupled with real-time rendering speed.

3. Method

Problem Formulation Given an input text prompt, our primary objective is to generate immersive 3D scenes that align with the given prompts. We choose to use 3D Gaus-

sians [19] as the foundational representations, due to their rapid inference speed, superior rendering quality, and explicit nature, which can significantly benefit a broad range of applications for the generated scenes. Specifically, each Gaussian is characterized by a set of parameters, including a center $\mathbf{x} \in \mathbb{R}^3$, a scaling factor $\mathbf{s} \in \mathbb{R}^3$, a quaternion $\mathbf{q} \in \mathbb{R}^4$, an opacity value $\alpha \in \mathbb{R}$, and a base color $\mathbf{c} \in \mathbb{R}^3$. Consequently, our goal is to generate a set of Gaussians, as described above, which optimally represents the scene.

While 3D Gaussians have proven effective in the realm of 3D reconstruction, the task of 3D scene generation presents new challenges. As noted in the original Gaussian Splatting study [19], the initial point clouds play a crucial role in the Gaussian training process. In their approach, a sparse reconstructed point cloud, acquired through COLMAP [41] from multi-view input, is used for initialization. However, such initial point clouds are not readily available for generation tasks. Another significant challenge arises from the lack of consistent dense supervisions. We formulate the Gaussians from sparser views with less consistent content. The task of achieving a robust 3D representation under such limited conditions poses formidable difficulties.

To address the aforementioned challenges, we propose a pipeline consisting of two primary stages, as depicted in Fig. 2. The initial stage involves the initialization for 3D Gaussians clouds, with the specifics detailed in Section 3.1. We adopt a strategy that utilizes a set of anchor cameras to incrementally build the point cloud, employing depth estimation and depth alignment modules. The subsequent stage entails refining 3D Gaussians using the initial Gaussians clouds with sparse supervision. We observe interesting training priors of 3D Gaussians, leveraging these to construct superior quality inpainted and super-resolved 3D Gaussians, as described in Section 3.2.

3.1. 3D Gaussians Initialization

To create an immersive scene, our initial step involves generating coarse Gaussians cloud representing the scene. This construction process starts from the initial view with camera extrinsic E_0 and progressively expands to incorporate other N anchor views, each with their respective extrinsics $\{E_1, E_2, \dots, E_N\}$. To simulate the experience of surrounded by immersive scenes as well as avoid the occlusions, our anchor cameras are only *rotated* from the initial view. We establish two underlying assumptions for our synthetic process. First, for simplicity, E_0 is defined as the identity matrix. Secondly, we assume that the cameras for all synthetic views share identical intrinsics K .

Initial View Generation: For the initial view, given the text prompt p , we employ the pretrained text-to-image generative model \mathcal{F} to generate the synthesized image I_0 . It's worth noting that a real image can also be utilized as the ini-

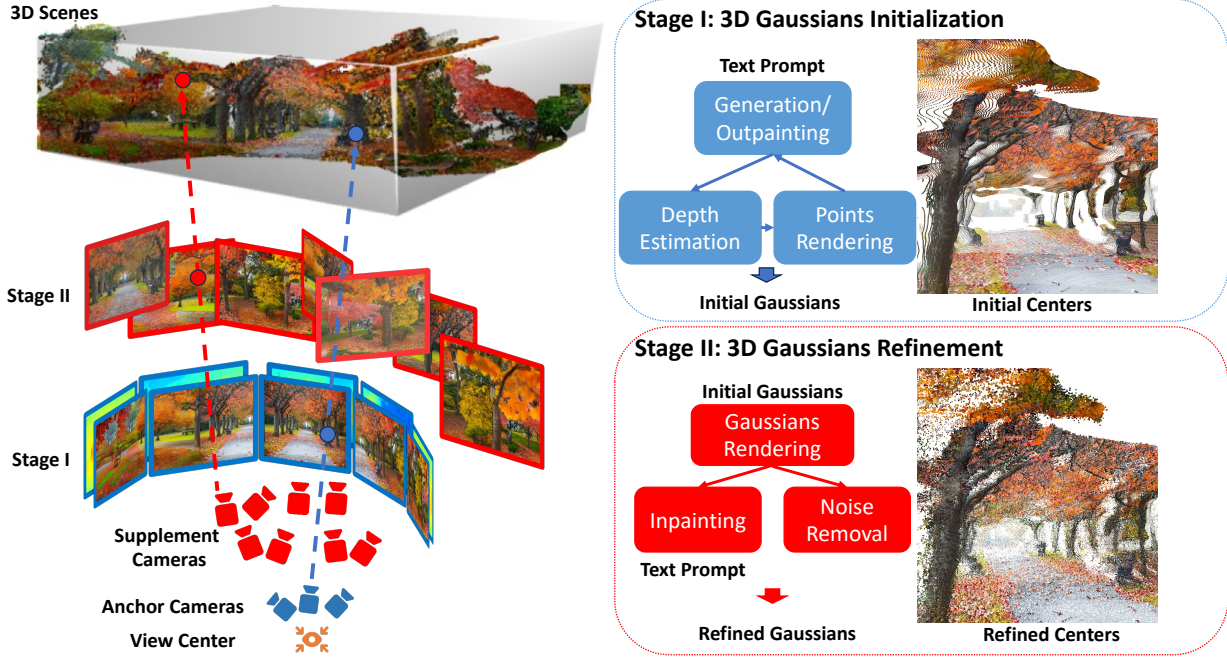


Figure 2. **The overview of our pipeline.** Our generation pipeline consists of two stages. In the first stage, we rotate the camera from the central view, and use diffusion models and monocular depth prediction modules to initialize a coarse Gaussian cloud. In the second stage, we sample more cameras around the center, and use diffusion-based inpainting modules to further refine the Gaussian cloud.

tial view. Further, we use the monocular depth estimation networks \mathcal{F}_{depth} to extract the depth map D_0 . Note that the field of view of our synthetic camera is set to the default value used in the depth estimation networks, which will reduce the estimation errors. This allows us to construct the initial points location using the formula:

$$P_0 = K^{-1} * E_0^{-1} * D_0, \quad (1)$$

where the operation $*$ applies to each pixel of D_0 .

Progressively Growing Starting with the initial points, we continue the process from the nearest camera sequentially until all the anchor cameras have been traversed. For each anchor camera, we first utilize the point cloud renderer \mathcal{R}_p to render the existing point cloud P_{i-1} for the current anchor view i . This process can be represented by the following equation:

$$V_i, M_i = \mathcal{R}_p(P_{i-1}, E_i, K), \quad (2)$$

where V_i denotes the rendered image and M_i represents the corresponding visibility mask. Subsequently, we generate the regions missing from the initial render by applying the outpainting models $\mathcal{F}_{outpaint}$ with the text prompt. This process enables us to achieve the synthesized image I_i for

the current view:

$$I_i = \mathcal{F}_{outpaint}(V_i, M_i). \quad (3)$$

The final step involves updating the existing points with newly generated points. We employ the same depth estimation network to estimate the depth of the synthesized image I_i , resulting in the depth map D_i . This estimated depth is aligned with the existing point cloud P_{i-1} by minimizing the error in the overlapping sections through a global scale and shift operation:

$$D'_i = \text{align}(\mathcal{F}_{depth}(I_i), P_{i-1}), \quad (4)$$

where the function align minimizes the error between the estimated depth and the existing point cloud.

The newly generated sections (i.e., areas corresponding to $1 - M_i$) are then projected into the world coordinate system and integrated into the point cloud. We update point cloud by:

$$P_i = \text{update}(P_{i-1}, D'_i, 1 - M_i), \quad (5)$$

where the function update projects the new parts onto the world coordinates and adds them to the point cloud. Please refer to the supplement for a detailed explanation of these operations.

Stretched Points Removal In our approach, depth is estimated using pretrained neural models, a process which may

occasionally result in common artifacts such as depth bleeding. This phenomenon typically occurs near object boundaries where there’s a drastic change in depth. As a consequence, the reconstructed point cloud may contain inaccurately stretched points along these boundaries. These erroneous points can significantly impede the refining procedure. As we’ll discuss in the following section, these incorrect points may generate additional errors due to the split-and-clone process. However, these stretched points are generally sparser than others. Therefore, we leverage K-nearest neighbors clustering in P_N to eliminate them. Specifically, we filter out the points where the nearest distance exceeds the average distance plus two standard deviations. This method effectively prunes the initial points, ensuring a more accurate and reliable refining procedure.

With the initial point cloud, we enhance the scene’s representation capability along with the rendering quality through the application of 3D Gaussians. Specifically, we utilize the point cloud to construct an initial Gaussian cloud. We align the centers of the Gaussians with the points and set the base color to match the color of the point cloud. Subsequently, the initial Gaussians G_0 are optimized using the sparse anchor views. Drawing from the observations made in the context of deep image priors [46], we discovered that implementing early stopping during training is especially effective at preventing the emergence of incorrect Gaussian shapes while also achieves visually-pleasing reconstruction results. This is particularly the case when supervision isn’t dense enough. As such, we limit the number of iterations during training to retrieve the optimized Gaussians G_1 for the initialization stage. This approach ensures a balance between training efficiency and the quality of the generated Gaussian shapes.

3.2. 3D Gaussians Refinement

As our anchor cameras are generated only by rotation but not translation, the generated scene contains a significant amount of missing regions, especially behind the generated objects in the foreground. Additionally, when the scene is zoomed in, the shape of the Gaussians becomes visible, leading to a noisy appearance in the rendering. We aim to fill in the missing regions and remove the noisy appearance during the refinement stage.

We augment the dataset by incorporating additional views, thereby ensuring robust rendering for regions occluded by foreground objects. In this stage, we sample an additional M_1 cameras with extrinsics of $E_{N+1}, E_{N+2}, \dots, E_{N+M_1}$ around the previous anchor cameras. These additional views serve to fill in the missing regions brought about by occlusion. For these augmented views, we abstain from updating the initial point cloud. This is due to the fact that the randomness of these views could potentially lead to highly inaccurate depth estimations, such

as those caused by extreme close objects. Instead, we leverage the split-and-clone process of the Gaussians to naturally cultivate new Gaussians. The split-and-clone process guarantees that the newly inpainted Gaussians appear near existing Gaussians and progressively expands outward from there (refer to the supplement for a detailed analysis). This feature enables us to inpaint 3D Gaussians using solely 2D supervision, as the initial position provides a strong prior, particularly useful for inpainting smooth surfaces. The synthesized image for a given view i can be computed using the following formula:

$$I_i = \mathcal{F}_{inpaint}(\mathcal{R}(G_1, E_i, K), M_i). \quad (6)$$

In this equation, $\mathcal{F}_{inpaint}$ is the inpainting networks applied to the rendered Gaussians $\mathcal{R}(G_1, E_i, K)$ and the mask M_i and i is in $[N + 1, N + M_1]$.

Following the inpainting stage, we proceed to sample additional cameras that zoom into the scene. This strategy aids in mitigating the issue of Gaussian noise when observing the scene closely. Leveraging the split-and-clone process allows 3D Gaussians to naturally adapt for super-resolution, thereby enabling them to accommodate fine details with ease. Similar to the inpainting process, we sample M_2 zoomed-in views with extrinsics $E_{N+M_1+1}, E_{N+M_1+2}, \dots, E_{N+M_1+M_2}$. By employing pretrained super-resolution and restoration structures, we can restore the image with a high level of detail. This augmentation further enhances the quality of the rendered scenes, ensuring more precise, detailed, and noise-free visualizations even at close range.

Training Objectives For optimization process in both stages, our optimization objective adheres to the same settings used in Gaussian Splatting [19], incorporating both the \mathcal{L}_1 loss and the D-SSIM loss. This is represented in the equation:

$$\mathcal{L} = \lambda \mathcal{L}_1 + (1 - \lambda) \mathcal{L}_{SSIM}, \quad (7)$$

where λ is the weight parameter that balances the contribution of the \mathcal{L}_1 loss and the D-SSIM loss to the final objective.

For the refinement stage, the training is supervised by all synthesized views $I_0, I_1, \dots, I_{N+M_1+M_2}$. The optimization duration for the refinement stage generally exceeds the initialization stage. However, we still employ early stopping to prevent the formulation of incorrect Gaussian shapes.

4. Experiments

4.1. Implementation Details

During the first stage, we employ ZoEDepth [3] for depth estimation and ControlNet [54] for outpainting; the initial optimization of 3D Gaussians is halted early at 1,000 iterations. We establish the angle difference between anchor

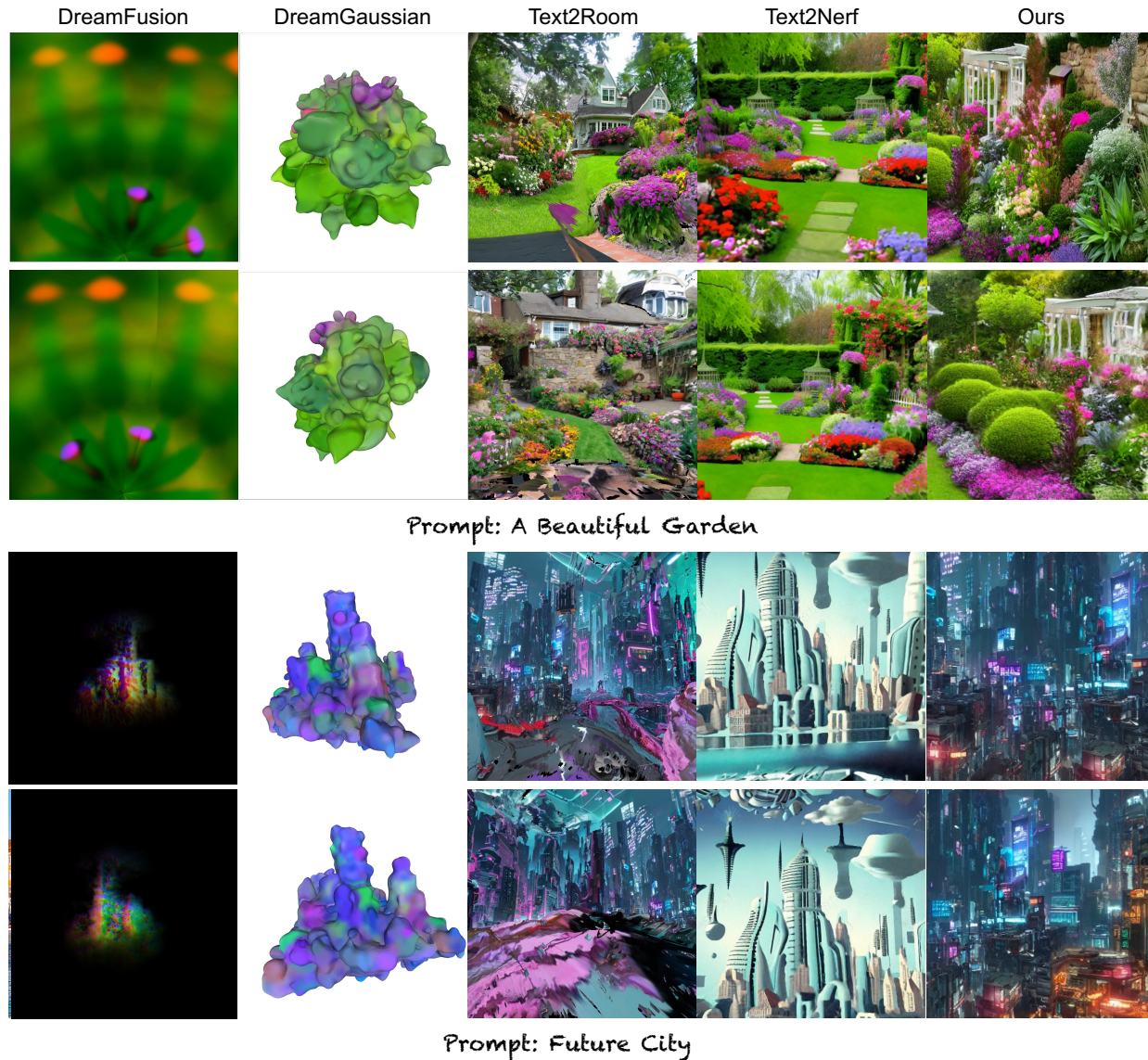


Figure 3. **Qualitative comparison with baselines** including DreamFusion [36], DreamGaussian [43], Text2Room [14], Text2Nerf [53] on the generation quality. We highly recommend that readers view the accompanying videos for a more thorough comparison.

cameras at 25 degrees and set the number of anchors between 7 and 16, contingent on the specific generation application. For the refinement stage, we utilize ControlNet [54] for inpainting and DiffBIR [23] for super-resolution. The refinement training is also given an early stop at 2,000 iterations. We sample between 3 to 6 cameras around each anchor and incorporate additional randomly sampled, zoomed-in views. Depending on the number of cameras sampled for refinement, it takes between 10 to 25 minutes to generate each scene on a single GPU. After the optimization process, the generated Gaussian can be rendered in real-time.

4.2. Comparison with Baselines

To assess the efficacy of our approach in the context of text-driven 3D scene generation, we compare with representative methods from three distinct categories. These include methods that employ SDS loss to distill 3D from pre-trained Diffusion models (e.g., DreamFusion [36]), methods that also use 3D Gaussians as underlying 3D representations (e.g., DreamGaussians [43]), and methods that utilize diffusion models to generate supervisions but employ alternate 3D representations (e.g., Text2Room [14] and Text2Nerf [53]).

Quantitative Comparison Given the absence of ground



Figure 4. **Diverse Output Generation:** Our pipeline is capable of synthesizing a variety of 3D scenes using the same prompts. We also demonstrate its ability to generate stylized scenes.

Method	BRISQUE ↓	NIQE ↓	CLIP ↑
DreamFusion [36]	67.0	12.0	22.6
DreamGaussian [43]	59.1	11.7	23.2
Text2Room [14]	28.4	5.41	28.1
Text2Nerf [53]	24.5	4.62	28.7
Ours	22.7	4.37	28.9

Table 1. **Quantitative Comparison with Baselines**

Stages	PSNR	SSIM	LPIPS
Initial	36.3	0.983	0.019
Refinement	35.1	0.982	0.023

Table 2. **Reconstruction Quality.** As our refinement stage includes more images for optimization, the metrics is slightly lower.

truth references for 3D scenes generated in relation to text prompts, conventional metrics such as PSNR and LPIPS [55] are not applicable for generation tasks. Nonetheless, we include PSNR, SSIM and LPIPS [55] values for the reconstruction of Gaussians as in Table. 2. The metrics prove the optimized Gaussians have already achieved high fidelity of reconstruction even with the early stop strategy. To assess the quality of the generated images, we follow the settings established in Text2Nerf [53], which employs BRISQUE [28] and the Natural Image Quality

Evaluator (NIQE) [29] to evaluate quality in the absence of a reference image. Additionally, we utilize the CLIP text-image similarity score [12, 37] to evaluate the degree of alignment between the rendered images and the input prompt. In both the image quality and alignment with text prompts, our method achieves the highest results. However, as these metrics may not provide a fully accurate representation, qualitative comparisons remain a crucial aspect of our evaluation process.

Qualitative Comparison We present qualitative comparison results with other baseline methods. As depicted in the Fig. 3, previous works like DreamFusion [36] which primarily focus on the generation of 3D objects underperforms in the context of scene generation, leading to blurry and less realistic textures. DreamGaussian utilize the 3D Gaussians as 3D representations but also works only on object-centric generation. When compared with Text2Room [14], our results capably handle outdoor scenes without noticeable gaps, owing to the high capacity of the Gaussians. Against Text2Nerf [53], our results achieve superior rendering quality, leading to more realistic scene generation. Note that as Text2Nerf has not been open-sourced yet, we directly use the released results with the same text prompts. However, image comparison does not capture 3D consistency. Therefore, we strongly recommend that readers refer to the supplementary videos for a more comprehensive comparison.

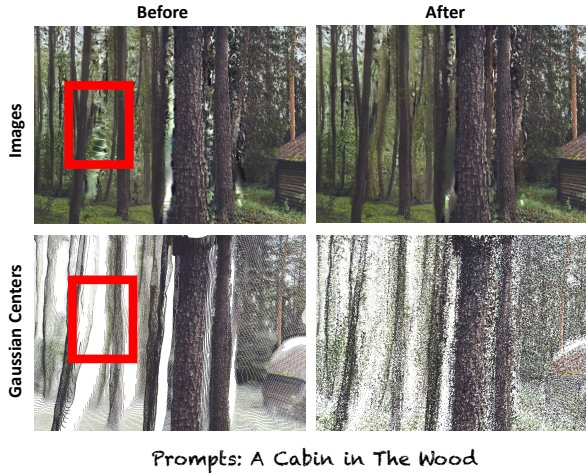


Figure 5. **Ablation study** on the refinement stage, which shows that the refinement helps filling in the missing regions and reducing the noisy appearance. After the refinement, the center of Gaussians effectively covering the original missing parts.



Figure 6. **Ablation study** on the initialization. Without using the anchor cameras, the generated images contain obvious gap.

4.3. Generation Capability

We showcase the high generation capacity and robustness of the proposed pipeline in the following three areas: **Diversity**: As depicted in the accompanying figures, our pipeline can generate a diverse array of photorealistic 3D scenes using the same text prompts as in Fig. 4. **Stylized and Imaginary Scenes**: As demonstrated in the figure, our approach is also capable of generating stylized and imaginary scenes in Fig. 4. **360 VR View**: Our method can further generate 360-degree views, suitable for VR scenes. The results are attached in the supplement.

4.4. Ablation Study

We conduct ablation studies to examine the design elements of our pipeline. Primarily, we are interested in investigating how refinement contributes to the enhancement of rendering quality and how the process of point initialization impacts the results. More ablations about early stop and removing stretched points are attached in the supplement.

Ablation on Refinement We examine the effectiveness of the refinement process as illustrated in the corresponding figures. In the absence of inpainting, it is observable that missing parts are filled with optimized Gaussians. With-

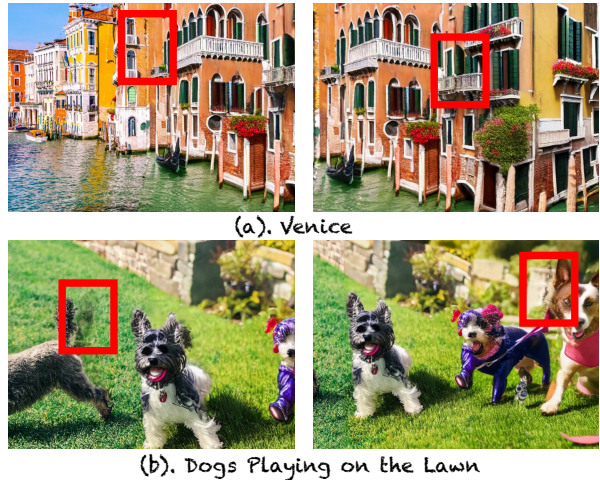


Figure 7. **Failure cases**. In (a), we demonstrate a scenario where an erroneous alignment results in noticeable gaps. In (b), we highlight an instance where the use of inpainting leads to undesirable ghosting effects.

out the restoration, the zoomed-in views are populated with Gaussian shapes, resulting in a noisy appearance. Following the refinement process, the rendered image exhibits enhanced cleanliness and clarity.

Ablation on Gaussian Initialization We explore the significance of 3D Gaussians initialization as in Fig. 6. If we initialize the Gaussian cloud directly using all views, as opposed to solely using the anchor views, the point cloud becomes disorganized, which subsequently impacts the quality of the generated Gaussians. The randomness of the viewing angle decrease the depth estimation accuracy especially for close views.

5. Limitation and Conclusion

In this study, we delve into the generation of immersive 3D scenes using 3D Gaussians. Our approach has yielded promising results, yet it has also revealed several challenges that necessitate further exploration. As depicted in Fig. 7, a key constraint of our method is the initial construction phase of the Gaussian cloud, which is heavily dependent on monocular depth estimation. Although depth alignment and subsequent Gaussian training can alleviate misalignment issues, significant estimation errors may still yield noticeable visual artifacts. Furthermore, the introduction of new objects during the refining stage can cause ghosting effects.

Nevertheless, despite these challenges, our proposed pipeline generally delivers high-fidelity 3D scene generation with 3D consistency, opening the door to various 3D applications. Future research is expected to enhance the results of inpainting 3D Gaussians, especially in cases where only 2D inputs are available.

References

- [1] Jonathan T Barron, Ben Mildenhall, Matthew Tancik, Peter Hedman, Ricardo Martin-Brualla, and Pratul P Srinivasan. Mip-nerf: A multiscale representation for anti-aliasing neural radiance fields. In *Proceedings of the IEEE/CVF International Conference on Computer Vision*, pages 5855–5864, 2021. 2
- [2] Matthew Berger, Andrea Tagliasacchi, Lee M Seversky, Pierre Alliez, Joshua A Levine, Andrei Sharf, and Claudio T Silva. State of the art in surface reconstruction from point clouds. In *35th Annual Conference of the European Association for Computer Graphics, Eurographics 2014-State of the Art Reports*, number CONF. The Eurographics Association, 2014. 2
- [3] Shariq Farooq Bhat, Reiner Birkel, Diana Wofk, Peter Wonka, and Matthias Müller. Zoedepth: Zero-shot transfer by combining relative and metric depth. *arXiv preprint arXiv:2302.12288*, 2023. 5, 11
- [4] Eric R Chan, Marco Monteiro, Petr Kellnhofer, Jiajun Wu, and Gordon Wetzstein. pi-gan: Periodic implicit generative adversarial networks for 3d-aware image synthesis. In *Proceedings of the IEEE/CVF conference on computer vision and pattern recognition*, pages 5799–5809, 2021. 3
- [5] Eric R Chan, Connor Z Lin, Matthew A Chan, Koki Nagano, Boxiao Pan, Shalini De Mello, Orazio Gallo, Leonidas J Guibas, Jonathan Tremblay, Sameh Khamis, et al. Efficient geometry-aware 3d generative adversarial networks. In *Proceedings of the IEEE/CVF Conference on Computer Vision and Pattern Recognition*, pages 16123–16133, 2022. 3
- [6] Yu Deng, Jiaolong Yang, Jianfeng Xiang, and Xin Tong. Gram: Generative radiance manifolds for 3d-aware image generation. In *Proceedings of the IEEE/CVF Conference on Computer Vision and Pattern Recognition*, pages 10673–10683, 2022. 2
- [7] Prafulla Dhariwal and Alexander Nichol. Diffusion models beat gans on image synthesis. *Advances in neural information processing systems*, 34:8780–8794, 2021. 3
- [8] Rafail Fridman, Amit Abecasis, Yoni Kasten, and Tali Dekel. Scenescape: Text-driven consistent scene generation. *arXiv preprint arXiv:2302.01133*, 2023. 2, 3
- [9] Ian Goodfellow, Jean Pouget-Abadie, Mehdi Mirza, Bing Xu, David Warde-Farley, Sherjil Ozair, Aaron Courville, and Yoshua Bengio. Generative adversarial networks. *Communications of the ACM*, 63(11):139–144, 2020. 3
- [10] Jiatao Gu, Alex Trevithick, Kai-En Lin, Joshua M Susskind, Christian Theobalt, Lingjie Liu, and Ravi Ramamoorthi. Nerfdiff: Single-image view synthesis with nerf-guided distillation from 3d-aware diffusion. In *International Conference on Machine Learning*, pages 11808–11826. PMLR, 2023. 3
- [11] Anchit Gupta, Wenhan Xiong, Yixin Nie, Ian Jones, and Barlas Oğuz. 3dgen: Triplane latent diffusion for textured mesh generation. *arXiv preprint arXiv:2303.05371*, 2023. 3
- [12] Jack Hessel, Ari Holtzman, Maxwell Forbes, Ronan Le Bras, and Yejin Choi. Clipscore: A reference-free evaluation metric for image captioning. *arXiv preprint arXiv:2104.08718*, 2021. 2, 7
- [13] Jonathan Ho, Ajay Jain, and Pieter Abbeel. Denoising diffusion probabilistic models. 2020. 3
- [14] Lukas Höllein, Ang Cao, Andrew Owens, Justin Johnson, and Matthias Nießner. Text2room: Extracting textured 3d meshes from 2d text-to-image models. In *Proceedings of the IEEE/CVF International Conference on Computer Vision*, 2023. 2, 3, 6, 7
- [15] Ajay Jain, Ben Mildenhall, Jonathan T. Barron, Pieter Abbeel, and Ben Poole. Zero-shot text-guided object generation with dream fields. In *Proceedings of the IEEE/CVF Conference on Computer Vision and Pattern Recognition (CVPR)*, pages 867–876, 2022. 3
- [16] Heewoo Jun and Alex Nichol. Shap-e: Generating conditional 3d implicit functions. *arXiv preprint arXiv:2305.02463*, 2023. 3
- [17] Animesh Karnewar, Andrea Vedaldi, David Novotny, and Niloy J Mitra. Holodiffusion: Training a 3d diffusion model using 2d images. In *Proceedings of the IEEE/CVF Conference on Computer Vision and Pattern Recognition*, pages 18423–18433, 2023. 3
- [18] Tero Karras, Samuli Laine, and Timo Aila. A style-based generator architecture for generative adversarial networks. In *Proceedings of the IEEE/CVF conference on computer vision and pattern recognition*, pages 4401–4410, 2019. 3
- [19] Bernhard Kerbl, Georgios Kopanas, Thomas Leimkühler, and George Drettakis. 3d gaussian splatting for real-time radiance field rendering. *ACM Transactions on Graphics (ToG)*, 42(4):1–14, 2023. 2, 3, 5
- [20] Han-Hung Lee and Angel X Chang. Understanding pure clip guidance for voxel grid nerf models. *arXiv preprint arXiv:2209.15172*, 2022. 3
- [21] Yiyi Liao, Katja Schwarz, Lars Mescheder, and Andreas Geiger. Towards unsupervised learning of generative models for 3d controllable image synthesis. In *Proceedings of the IEEE/CVF conference on computer vision and pattern recognition*, pages 5871–5880, 2020. 3
- [22] Chen-Hsuan Lin, Jun Gao, Luming Tang, Towaki Takikawa, Xiaohui Zeng, Xun Huang, Karsten Kreis, Sanja Fidler, Ming-Yu Liu, and Tsung-Yi Lin. Magic3d: High-resolution text-to-3d content creation. In *Proceedings of the IEEE/CVF Conference on Computer Vision and Pattern Recognition*, pages 300–309, 2023. 3
- [23] Xinqi Lin, Jingwen He, Ziyang Chen, Zhaoyang Lyu, Ben Fei, Bo Dai, Wanli Ouyang, Yu Qiao, and Chao Dong. Diffbir: Towards blind image restoration with generative diffusion prior. *arXiv preprint arXiv:2308.15070*, 2023. 6
- [24] Minghua Liu, Chao Xu, Haian Jin, Linghao Chen, Zexiang Xu, Hao Su, et al. One-2-3-45: Any single image to 3d mesh in 45 seconds without per-shape optimization. *arXiv preprint arXiv:2306.16928*, 2023. 3
- [25] Ruoshi Liu, Rundi Wu, Basile Van Hoorick, Pavel Tokmakov, Sergey Zakharov, and Carl Vondrick. Zero-1-to-3: Zero-shot one image to 3d object. In *Proceedings of the IEEE/CVF International Conference on Computer Vision*, pages 9298–9309, 2023. 3
- [26] Stephen Lombardi, Tomas Simon, Jason Saragih, Gabriel Schwartz, Andreas Lehrmann, and Yaser Sheikh. Neural vol-

- umes: Learning dynamic renderable volumes from images. *arXiv preprint arXiv:1906.07751*, 2019. 2
- [27] Ben Mildenhall, Pratul P Srinivasan, Matthew Tancik, Jonathan T Barron, Ravi Ramamoorthi, and Ren Ng. Nerf: Representing scenes as neural radiance fields for view synthesis. *Communications of the ACM*, 65(1):99–106, 2021. 2, 3
- [28] Anish Mittal, Anush Krishna Moorthy, and Alan Conrad Bovik. No-reference image quality assessment in the spatial domain. *IEEE Transactions on image processing*, 21(12):4695–4708, 2012. 7
- [29] Anish Mittal, Rajiv Soundararajan, and Alan C Bovik. Making a “completely blind” image quality analyzer. *IEEE Signal processing letters*, 20(3):209–212, 2012. 7
- [30] Nasir Mohammad Khalid, Tianhao Xie, Eugene Belilovsky, and Tiberiu Popa. Clip-mesh: Generating textured meshes from text using pretrained image-text models. In *SIGGRAPH Asia 2022 conference papers*, pages 1–8, 2022. 3
- [31] Norman Müller, Yawar Siddiqui, Lorenzo Porzi, Samuel Rota Buló, Peter Kotschieder, and Matthias Nießner. Diffri: Rendering-guided 3d radiance field diffusion. In *Proceedings of the IEEE/CVF Conference on Computer Vision and Pattern Recognition*, pages 4328–4338, 2023. 3
- [32] Jacob Munkberg, Jon Hasselgren, Tianchang Shen, Jun Gao, Wenzheng Chen, Alex Evans, Thomas Mueller, and Sanja Fidler. Extracting Triangular 3D Models, Materials, and Lighting From Images. *arXiv:2111.12503*, 2021. 2
- [33] Thu Nguyen-Phuoc, Chuan Li, Lucas Theis, Christian Richardt, and Yong-Liang Yang. Hologan: Unsupervised learning of 3d representations from natural images. In *Proc. ICCV*, 2019. 2
- [34] Michael Niemeyer and Andreas Geiger. Giraffe: Representing scenes as compositional generative neural feature fields. In *Proceedings of the IEEE/CVF Conference on Computer Vision and Pattern Recognition*, pages 11453–11464, 2021. 3
- [35] Roy Or-El, Xuan Luo, Mengyi Shan, Eli Shechtman, Jeong Joon Park, and Ira Kemelmacher-Shlizerman. Stylesdf: High-resolution 3d-consistent image and geometry generation. In *Proceedings of the IEEE/CVF Conference on Computer Vision and Pattern Recognition*, pages 13503–13513, 2022. 3
- [36] Ben Poole, Ajay Jain, Jonathan T Barron, and Ben Mildenhall. Dreamfusion: Text-to-3d using 2d diffusion. In *The Eleventh International Conference on Learning Representations*, 2022. 2, 3, 6, 7
- [37] Alec Radford, Jong Wook Kim, Chris Hallacy, Aditya Ramesh, Gabriel Goh, Sandhini Agarwal, Girish Sastry, Amanda Askell, Pamela Mishkin, Jack Clark, et al. Learning transferable visual models from natural language supervision. In *International conference on machine learning*, pages 8748–8763. PMLR, 2021. 3, 7
- [38] Chris Rockwell, David F Fouhey, and Justin Johnson. Pixel-synth: Generating a 3d-consistent experience from a single image. In *Proceedings of the IEEE/CVF International Conference on Computer Vision*, pages 14104–14113, 2021. 3
- [39] Robin Rombach, Andreas Blattmann, Dominik Lorenz, Patrick Esser, and Björn Ommer. High-resolution image synthesis with latent diffusion models. In *Proceedings of the IEEE/CVF conference on computer vision and pattern recognition*, pages 10684–10695, 2022. 2, 3
- [40] Chitwan Saharia, William Chan, Saurabh Saxena, Lala Li, Jay Whang, Emily L Denton, Kamyar Ghasemipour, Raphael Gontijo Lopes, Burcu Karagol Ayan, Tim Salimans, et al. Photorealistic text-to-image diffusion models with deep language understanding. 2022. 3
- [41] Johannes L Schonberger and Jan-Michael Frahm. Structure-from-motion revisited. In *Proceedings of the IEEE conference on computer vision and pattern recognition*, pages 4104–4113, 2016. 3
- [42] Jiaming Song, Chenlin Meng, and Stefano Ermon. Denoising diffusion implicit models. *arXiv preprint arXiv:2010.02502*, 2020. 3
- [43] Jiayang Tang, Jiawei Ren, Hang Zhou, Ziwei Liu, and Gang Zeng. Dreamgaussian: Generative gaussian splatting for efficient 3d content creation. *arXiv preprint arXiv:2309.16653*, 2023. 2, 3, 6, 7
- [44] Junshu Tang, Tengfei Wang, Bo Zhang, Ting Zhang, Ran Yi, Lizhuang Ma, and Dong Chen. Make-it-3d: High-fidelity 3d creation from a single image with diffusion prior. *arXiv preprint arXiv:2303.14184*, 2023. 3
- [45] Richard Tucker and Noah Snavely. Single-view view synthesis with multiplane images. In *The IEEE Conference on Computer Vision and Pattern Recognition (CVPR)*, 2020. 2
- [46] Dmitry Ulyanov, Andrea Vedaldi, and Victor Lempitsky. Deep image prior. In *Proceedings of the IEEE conference on computer vision and pattern recognition*, pages 9446–9454, 2018. 2, 5
- [47] Haochen Wang, Xiaodan Du, Jiahao Li, Raymond A Yeh, and Greg Shakhnarovich. Score jacobian chaining: Lifting pretrained 2d diffusion models for 3d generation. In *Proceedings of the IEEE/CVF Conference on Computer Vision and Pattern Recognition*, pages 12619–12629, 2023. 3
- [48] Tengfei Wang, Bo Zhang, Ting Zhang, Shuyang Gu, Jianmin Bao, Tadas Baltrusaitis, Jingjing Shen, Dong Chen, Fang Wen, Qifeng Chen, et al. Rodin: A generative model for sculpting 3d digital avatars using diffusion. In *Proceedings of the IEEE/CVF Conference on Computer Vision and Pattern Recognition*, pages 4563–4573, 2023. 3
- [49] Daniel Watson, William Chan, Ricardo Martin-Brualla, Jonathan Ho, Andrea Tagliasacchi, and Mohammad Norouzi. Novel view synthesis with diffusion models. *arXiv preprint arXiv:2210.04628*, 2022. 3
- [50] Olivia Wiles, Georgia Gkioxari, Richard Szeliski, and Justin Johnson. Synsin: End-to-end view synthesis from a single image. In *Proceedings of the IEEE/CVF Conference on Computer Vision and Pattern Recognition*, pages 7467–7477, 2020. 3
- [51] DeJia Xu, Yifan Jiang, Peihao Wang, Zhiwen Fan, Yi Wang, and Zhangyang Wang. Neurlift-360: Lifting an in-the-wild 2d photo to a 3d object with 360deg views. In *Proceedings of the IEEE/CVF Conference on Computer Vision and Pattern Recognition*, pages 4479–4489, 2023. 3

- [52] Taoran Yi, Jiemin Fang, Guanjun Wu, Lingxi Xie, Xiaopeng Zhang, Wenyu Liu, Qi Tian, and Xinggang Wang. Gaussian-dreamer: Fast generation from text to 3d gaussian splatting with point cloud priors. *arXiv preprint arXiv:2310.08529*, 2023. 2
- [53] Jingbo Zhang, Xiaoyu Li, Ziyu Wan, Can Wang, and Jing Liao. Text2nerf: Text-driven 3d scene generation with neural radiance fields. *arXiv preprint arXiv:2305.11588*, 2023. 2, 3, 6, 7
- [54] Lvmin Zhang, Anyi Rao, and Maneesh Agrawala. Adding conditional control to text-to-image diffusion models, 2023. 5, 6, 11
- [55] Richard Zhang, Phillip Isola, Alexei A Efros, Eli Shechtman, and Oliver Wang. The unreasonable effectiveness of deep features as a perceptual metric. In *Proceedings of the IEEE conference on computer vision and pattern recognition*, pages 586–595, 2018. 7

Appendix

The supplementary materials are organized as follows: Initially, we delve into the specifics of our implementation, detailing the training settings and the construction of the point-cloud. Following this, we execute a more comprehensive analysis of several issues identified in the paper. Finally, we present additional results, featuring a diverse range of text prompts.

A. Implementation Details

A.1. Model Details

For Gaussian training, we initialize the opacity at 0.5 and set the initial shape as a sphere. We’ve observed that the training of 3D is significant. The image width and height are configured at 704 and 512, respectively. Adhering to the original settings in Gaussian splatting, the learning rate of opacity is established at 0.05, scaling at 0.005, and rotation at 0.001. The split and clone process is triggered every 100 iterations.

During the inpainting and outpainting process, in the initial stage, we set the mask dilation pixels to 14 and adjust it to 5 for the refinement stage. For ControlNet [54], we set the scale at 9 and the control strength at 1. The guess mode is deactivated and the generation step is set to 20.

Following the configuration in ZoEDepth [3], where the field of view is set to an angle of 55 degrees, we adopt these settings for the intrinsics of our synthetic cameras.

A.2. Depth Alignment

In this section, we delve deeper into the process of depth alignment, an integral part of our methodology. The final step in our procedure involves a crucial update where the existing points are updated with newly generated ones. This

step requires attention as it involves aligning the newly estimated depth map, represented as D , with the pre-existing components of the model.

A crucial aspect of this process is the minimization of error in the overlapping regions. These areas, where the new points intersect with the existing ones, can be particularly prone to discrepancies. By focusing on these overlapping parts, we aim to optimize the alignment and, by extension, the overall quality of the resulting model. To achieve this alignment, we estimate two key parameters: the global scale s , and the global depth shift b . The global scale s refers to the factor by which we adjust the depth values of the new points to match the scale of the existing model. On the other hand, the global shift b corresponds to the uniform adjustment required to align the depth values of the new points with those of the existing ones. To determine the optimal values of s and b that minimize the error in the overlapping regions, we frame this as a least squares problem. The method involves finding the values of s and b that minimize the sum of the squares of the differences between the estimated and actual depth values in the overlapping regions.

We compute s and b using the following least squares formulas:

$$s = \frac{n \sum DD_0 - \sum D \sum D_0}{n \sum D^2 - (\sum D)^2}$$

$$b = \frac{\sum D_0 - s \sum D}{n},$$

where n is the total number of the points, and D_0 is the original depth. The depth after the alignments becomes:

$$D' = sD + b$$

B. Analysis

We carry out additional experiments to delve into three aspects: an ablation study examining the impact of removing stretched points during initialization, an investigation into the position of newly added Gaussians via the split-and-clone method, and a comparison study to assess the effect of applying early stopping.

B.1. Removing Stretched Points

During the initialization phase, we discard the stretched points because their incorrect initial positions could potentially degrade the quality of the inpainting results. Fig. 9 demonstrates that the removal of these points results in a clearer inpainted region.

B.2. Analysis on Split-and-Clone

We’ve observed a notable pattern with the split-and-clone operation in Gaussian Splatting. Each Gaussian is tracked



Figure 8. 360 Scenes..

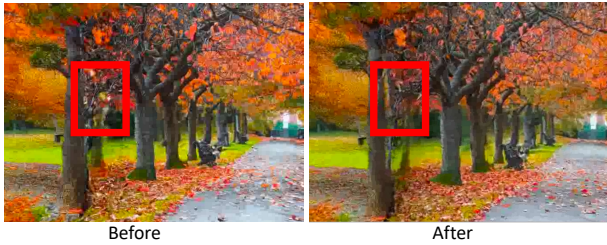


Figure 9. Comparison on Removing Stretched Points.

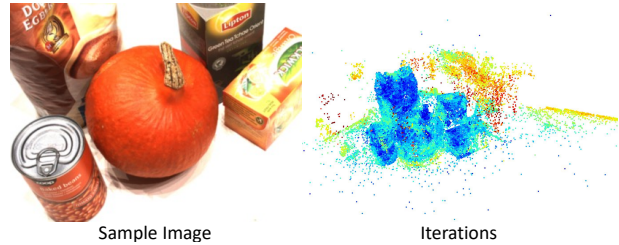


Figure 10. Analysis on the Newly Splitted Points..

with an additional parameter that records the iteration of splitting. If a Gaussian splits at the N th iteration, this parameter is recorded as $N + 1$. As depicted in Fig. 10, the blue color represents initial points. The redder a point becomes, the higher its iteration number. It can be seen that the points split progressively from near to far. With this pattern in place, assuming the initial points are correct, newly added points will be positioned around the existing surface. This characteristic is advantageous during training when only sparse 2D supervision is available.

B.3. Comparison on Early Stop

We present a comparison of results with and without the implementation of early stopping. As illustrated in Fig. 11, the accuracy of the Gaussian shapes degrades when early stopping is not applied.

C. More Results

In this section, we include additional results generated using our proposed Text2Immersion pipeline. We also provide videos that better illustrate the 3D consistency. We strongly encourage readers to examine these materials.



Figure 11. Analysis on Early Stop..

C.1. More Results with Diverse Text Prompt

We provide more results with diverse text prompt in Fig. 12.

C.2. 360 Scenes

We also show the 360 scenes Fig. 8.



Japanese Style Room



Train Station



A Cozy Living Room



A Clean Kitchen

Figure 12. More results..